ACTA IMEKO
February 2015, Volume 4, Number 1, 44 – 52
www.imeko.org

Statistical characterization of the 2.45 GHz propagation channel aboard trains

Annalisa Liccardo [1], Andrea Mariscotti [2], Attilio Marrese [1], Nicola Pasquino [1], Rosario Schiano Lo Moriello [1]

[1] *Dept. of Electrical Engineering and Information Technologies, University of Naples Federico II, Via Claudio 21, Naples Italy*
[2] *Dept. of Naval and Electrical Engineering, University of Genoa, Via all'Opera Pia 11, Genoa Italy*

ABSTRACT
The propagation channel aboard trains is investigated with reference to the propagation path loss within cars, the delay spread and the coherence bandwidth. Results show that the path loss exponent is slightly smaller than in free space, possibly due to reflections by metal walls, and that it does not depend significantly on the position of transmitter and receiver. The delay spread and coherence bandwidth depend on both the polarization and distance between transmitter and receiver while the effect of interaction is not statistically significant. The best fit for both delay spread's and coherence bandwidth's experimental distribution is also investigated. Results show that it does not always match models suggested in the literature and that the fit changes with the values of the input parameters. Finally, the functional law between coherence bandwidth and delay spread is determined. Results typically match expectations although the specific measurement configuration effects the model parameters.

Section: RESEARCH PAPER

Keywords: radio propagation channel; path loss; multipath propagation; delay spread; coherence bandwidth; statistical analysis of measurement data

Citation: A. Liccardo, A. Mariscotti, A. Marrese, N. Pasquino, R. Schiano Lo Moriello, Statistical characterization of the 2.45 GHz propagation channel aboard Trains, Acta IMEKO, vol. 4, no. 1, article 8, February 2015, identifier: IMEKO-ACTA-04 (2015)-01-08

Editor: Paolo Carbone, University of Perugia

Received December 13th, 2013; **In final form** November 17th, 2014; **Published** February 2015

Funding: This work was supported by Measurement Science Consultancy, The Netherlands

Corresponding author: Nicola Pasquino, e-mail: npasquin@unina.it

1. INTRODUCTION

Use of telecommunication services aboard trains is becoming more and more common for providing information and entertainment services to passengers during trips. Recently, WiFi access points began to be installed on board with the aim of providing passengers with wide-band access to the Internet. Trains are a possibly harsh environment to wireless propagation, given the presence of metal walls, seats, moving and steady passengers, besides emissions due to electric and electronic equipment and the power quality phenomena that may cause interference with electronic devices [1]. There are two main areas of interest for researchers in order to reduce performance degradation: the study of the propagation characteristics aboard trains to determine the attenuation

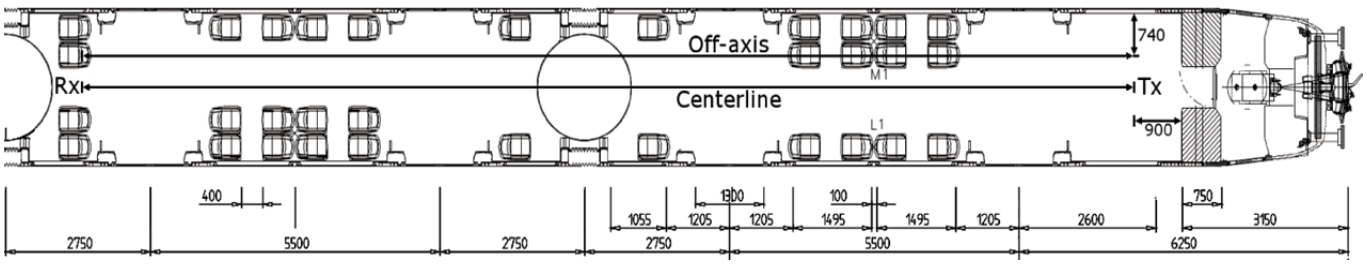

Figure 1. Train layout.

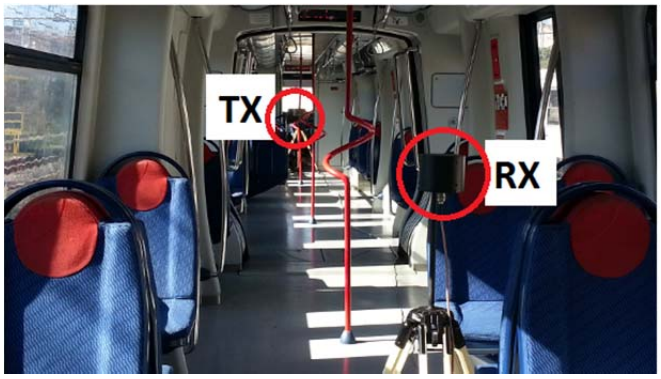

Figure 2. Measurement setup.

law and multipath properties, and the investigation of the effects of external disturbance onto the telecommunication signal. In [2]–[4] the results of an extensive measurement campaign to characterize the behavior of the disturbance radiated by the electric arc generated by the interaction between pantograph and overhead wire can be found, while the effects of pulses onto some Quality-of-Service parameters have been investigated in [5].

With reference to the characterization of the propagation channel, literature about this topic usually includes research papers about the propagation in different scenarios and at different frequencies. In [6], [7] it is shown that the use of a directive antenna reduces the Doppler spread and increases the received power when train runs towards the base transmitting station (BTS); when train moves away from BTS the omnidirectional antenna provides better results instead. In [8]–[11] it is shown that the classical models for propagation loss (such as Hata model and two-ray model) are inadequate for attenuation prediction when propagation occurs under the effect of structures like viaducts and terrain cuttings (canyons). Moreover, the presence of canyons, especially if topped by bridges, determines higher path losses than in the case of viaducts. With specific reference to propagation on board, in [12], [13] a narrow-band approach has shown that the transmitted signal can re-enter cars through windows and that its contribution to inter-car propagation is more relevant than the line-of-sight (LOS) signal. In [14] propagation on board has been analyzed with a 2.35 GHz continuous-wave signal and both a planar and an omnidirectional antenna, placed at different locations. The path loss and the Ricean K-factor are shown to be related to the antenna type, while the delay spread is independent of the measurement configuration. Studies performed aboard ships [15]–[18] only partially can be applied to trains due to differences in the geometrical and electromagnetic configurations.

The paper is organized as follows: in Section II the measurement setup and methodology for the experimental studies are described; in Section III the results are presented.

2. MEASUREMENT SETUP

Measurements were run on an ETR200 train owned by Circumvesuviana s.r.l., an Italian local transportation service. Figure 1 shows a portion of the train layout, with dimension in millimeters.

The properties of the propagation channel were investigated with a narrow-band approach. The transmitting port of a FieldFox N9918A Vector Network Analyzer by Agilent has been connected to a BBHA 9120D horn antenna by Schwarzbeck, while the receiving port to an EM6865 biconical antenna by Electrometrics. Automated calibration was run to normalize the attenuation introduced by cables and connections. Also, care has been taken to keep polarization coupling and to maximize the received signal by a proper antenna alignment. It was not necessary to take into account antenna factors because the main focus has been on the propagation loss exponent and not on the absolute value of loss itself. Measurements were executed in a steady train, without significant reflectors in close proximity outside the car. Figure 1 also shows distances from the wall (in mm) for the two propagation configurations for path loss measurements, which were taken along the centerline of the car and away from it (off-axis measurements), both at 120 cm height. Samples were taken moving the receiving antenna away from the transmitting one starting at 1 m up to 20 m in 10 cm steps. Figure 2 shows a view of the propagation environment for centerline measurements. It is apparent that propagation is affected by reflection on the walls, seats and vertical handrails, because of which the number of measurement points was reduced from 190 to

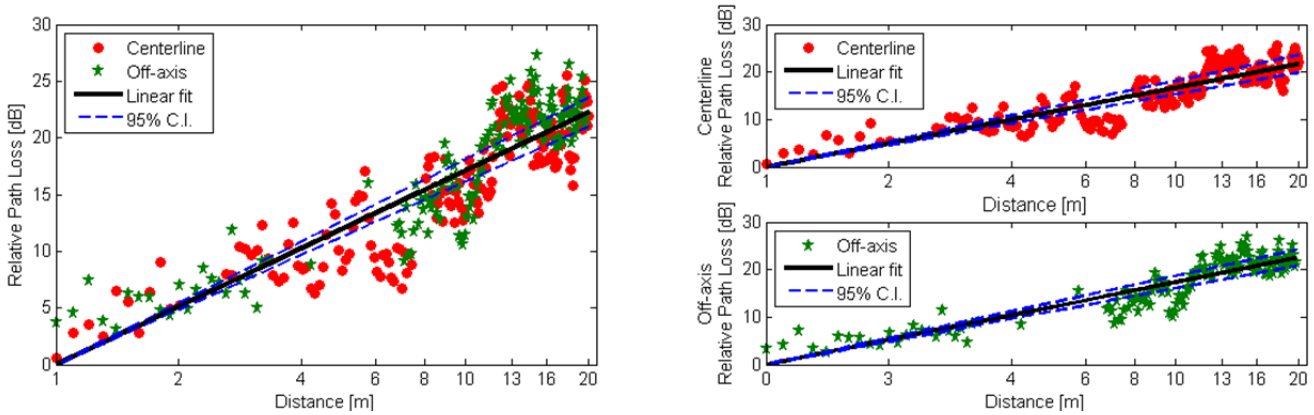

Figure 3. Path loss measurements and regression with 95% confidence intervals. Left: centerline and off-axis; upper right: centerline; lower right: off-axis.

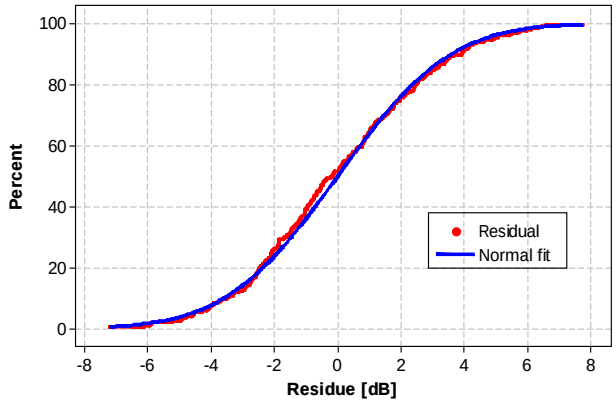

a) Residuals of the whole set of propagation measurement data

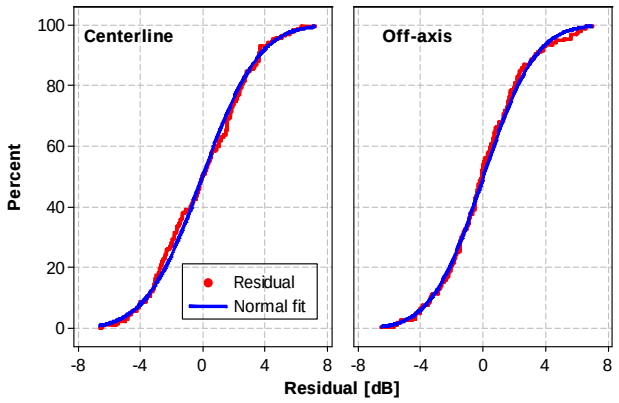

b) Residuals for centerline and off-axis propagation

Figure 4. Residuals of regression.

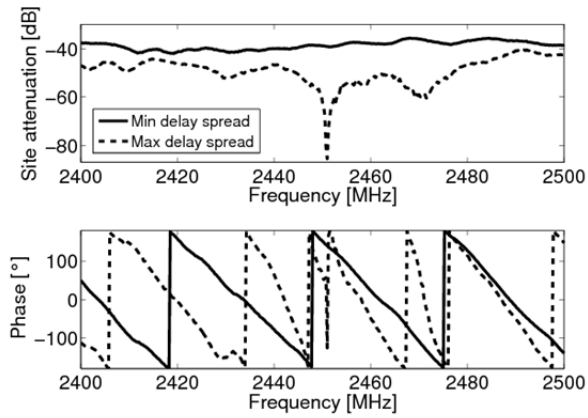

a) Magnitude and phase frequency response for minimum and maximum delay spread propagation

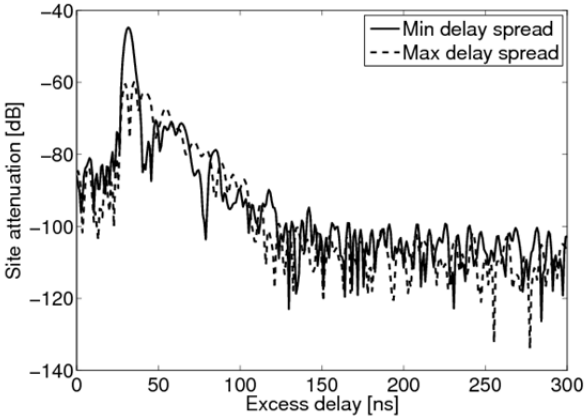

b) Impulse response for minimum and maximum delay spread propagation

Figure 5. Frequency and impulse response.

171 and 151 for the centerline and off-axis configuration, respectively.

Delay spread was measured along the centerline, both in vertical and horizontal polarization, at 120 cm height and three distances, i.e. 5, 10 and 15 m, moving the whole system at 10 cm steps. Again, some measurement points were missed, this time because of the presence of seats along the off-axis positions besides the ones already excluded because of the handrails.

3. RESULTS

3.1. Relative path loss PL_r

Since Internet access on board is expected to be granted through WiFi access points, channel propagation has been investigated in the 2.45 GHz band. Figure 3 shows the relative path loss PL_r obtained by normalizing the received power to that measured at 1 m from the transmitting antennas [19], [20]. The graph on the left shows both centerline and off-axis samples, and regression is carried out without distinction between the two configurations. Variability about the regression line is typically caused by the external noise affecting the measurement setup [21]. Because of the inhomogeneity of the propagation environment (see Figure 1), different exponents are expected to rule the power-decay law along the channel. Therefore the approach shown in [22] should have been adopted. However, the limited number of points assigned to each propagation layer would have resulted in a reduced significance of the regression analysis. For this reason, no distinction was made, and the exponent n can be thought of as the average one over the whole distance.

The model for the relative path loss PL_r is [23]:

$$PL_r(d) = 10n\log\left(d/d_0\right) + X \quad (1)$$

where d_0 = 1 m is the reference distance and X is a random variable describing the effect of multipath propagation onto received power, expected to be distributed according to a Gaussian random variable.

With the obtained experimental data, the path loss

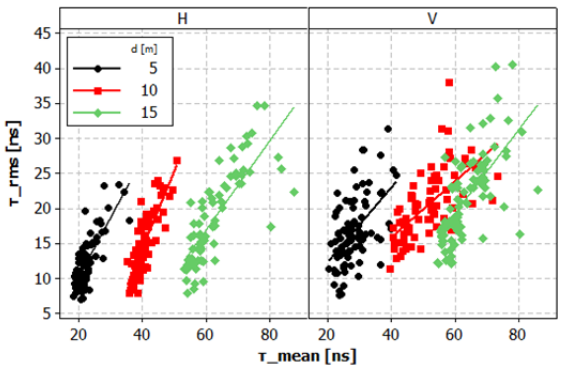

Figure 6. τ_{rms} vs $\overline{\tau}$ for each combination of input factors.

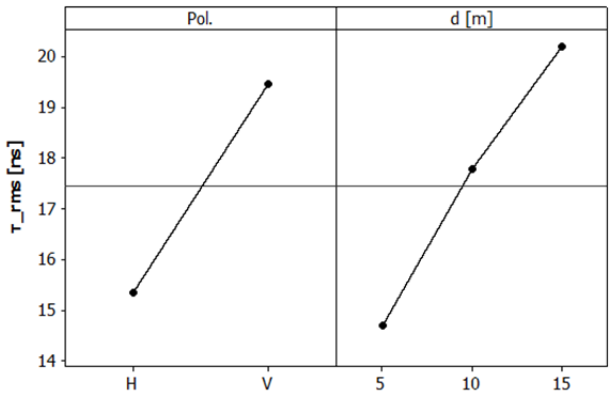

a) Main effects plot of polarization and distance for τ_{rms}

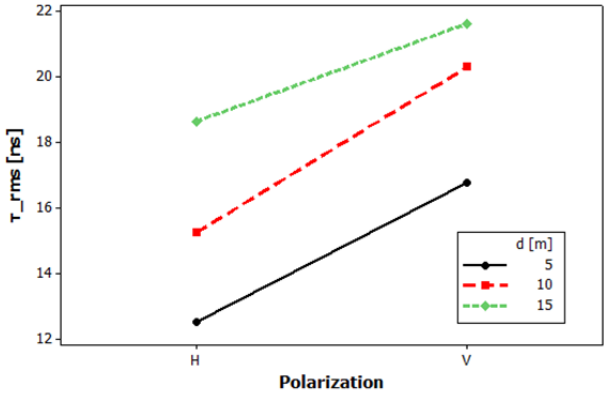

b) Interaction plot between polarization and distance for τ_{rms}

Figure 7. Main effects and interaction plots for τ_{rms}.

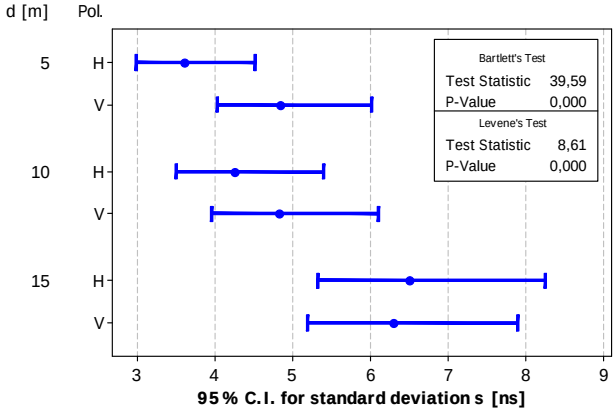

a) 95% confidence interval for standard deviation

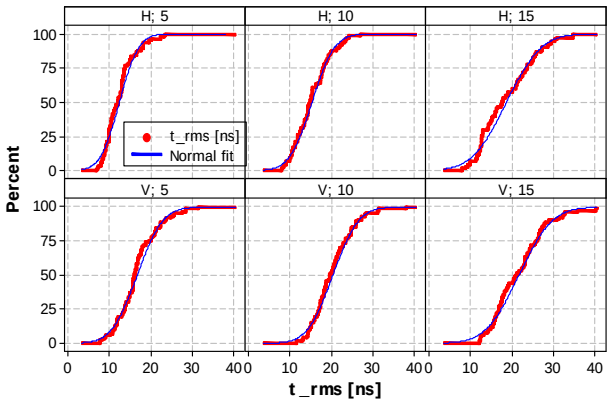

b) Experimental CDF's and normal fit

Figure 8. Validation of ANOVA hypothesis for τ_{rms}.

exponent turns out to be n = 1.71, smaller than that for free-space due to reflection on metal walls. To check that differences between the two propagation directions were indeed statistically insignificant, we also applied the regression procedure separately to the two propagation scenarios. The exponent for centerline and off-axis measurements turned out to be n_c = 1.67 and n_o = 1.73 respectively. The associated 95% confidence intervals are shown in Table **1**. Because of the overlap between them and with the confidence interval for the indistinct regression, propagation in the two configurations can be assumed to be very similar.

Figure 4 shows that the Gaussian model fits the experimental distribution of residuals from linear regression as expected by model (1). Residuals from the whole set of propagation data ("overall" propagation) are Normal with a p-value p = 10% (Figure 4.a), while p = 12.7% and p > 15% for centerline and off-axis propagation, respectively. Mean values of residuals are zero with p = 99.7%, p = 85.6% and p = 68.1% for the whole measurement set, centerline and off-axis propagation respectively. The 95% confidence intervals for the mean values are [-0.304;0.305], [-0.39;0.47] and [-0.50;0.33] respectively. Moreover, we cannot reject the hypothesis of equal variances for the centerline and off-axis scenarios unless we accept a risk at least equal to 29.1%. The 95% confidence interval for the ratio of the two variances is [0.87;1.61].

Table 1. Path loss exponent's 95% confidence intervals.

n, overall	n_c, centerline	n_o, off-axis
[1.61;1,81]	[1.53;1.81]	[1.60;1.86]

3.2. Frequency and impulse response

Figure 5.a shows the frequency response (magnitude and phase) of the propagation channel for horizontal polarization with 10 m separation. In the figure the responses with the smallest and largest τ_{rms} delay spread, calculated according to [23] and described in the next section, are plotted. The square magnitude of the associated impulse responses are plotted in Figure 5.b.

3.3. *rms* delay spread τ_{rms}

The mean excess delay $\bar{\tau}$ and the *rms* delay spread τ_{rms} are quantities used to estimate the time dispersion properties of the multipath channel.

The mean excess delay $\bar{\tau}$ is the first central moment of the power delay profile:

$$\bar{\tau} = \frac{\sum_k P(\tau_k)\tau_k}{\sum_k P(\tau_k)} \tag{2}$$

while the rms delay spread τ_{rms} is defined as the square root of the second central moment of the power delay profile:

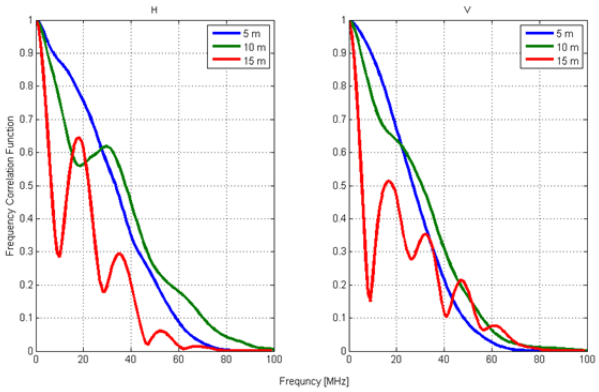

Figure 9. Frequency correlation functions.

$$\tau_{rms} = \sqrt{\overline{\tau^2} - \left(\overline{\tau}\right)^2} \tag{3}$$

where $\overline{\tau^2}$ is the mean square value:

$$\overline{\tau^2} = \frac{\sum_k P(\tau_k)\tau_k^2}{\sum_k P(\tau_k)} \tag{4}$$

Table 2 shows the sample mean values and the sample variance for τ_{rms} and $\overline{\tau}$. For both parameters the mean value increases with separation between antennas, but for the mean excess delay the increment has a larger magnitude.

The relation between *rms* delay spread and mean excess delay, shown in Figure 6, is linear and follows the model:

$$\tau_{rms} = \alpha + \beta \times \overline{\tau}\,, \tag{5}$$

where it can also be seen that for vertical polarization the correlation coefficient ρ is usually smaller: its values are 76.2%, 80.3% and 78,9% for 5, 10, 15 m horizontal polarization and 53.7%, 65.0% and 66.7% for the same distances, vertical polarization. Table 3 reports the values of the α and β parameters.

Figure 7.a shows the main effects of distance and polarization on τ_{rms}, while Figure 7.b shows the interaction plot between the two quantities. Figure 7.a shows that on average, the two polarizations cause a significant change in the amplitude of τ_{rms}, namely the vertical polarization typically suffers from a larger contribution from secondary peaks of the impulse response, that is reflection contributions are more numerous or present higher amplitudes. This may be due to the different boundary conditions encountered by vertically and horizontally polarized waves. The plot on the right of Figure 7.a shows that at greater distances the delay spread increases on average, which is due to the larger number of reflected signals arriving at the receiving antenna. The interaction plot in Figure 7.b is used to determine if the effect of polarization also depends on distance. It can be seen that the increase in the delay spread when the distance changes between 5 m and 15 m is different for the two polarizations. The interaction plot therefore seems to indicate that there is indeed interaction between the two factors.

For a more complete analysis, the analysis of variance (ANOVA) was run on experimental data. Results show

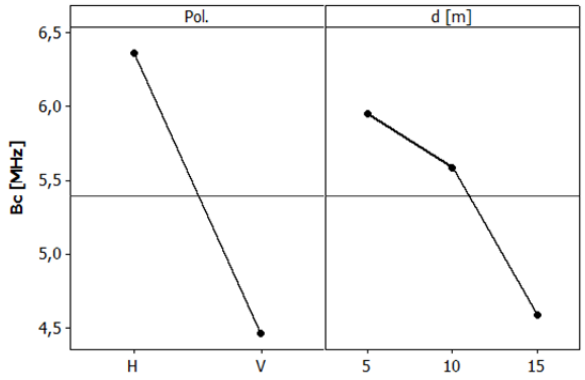

a) Main effects plot of polarization and distance for B_c

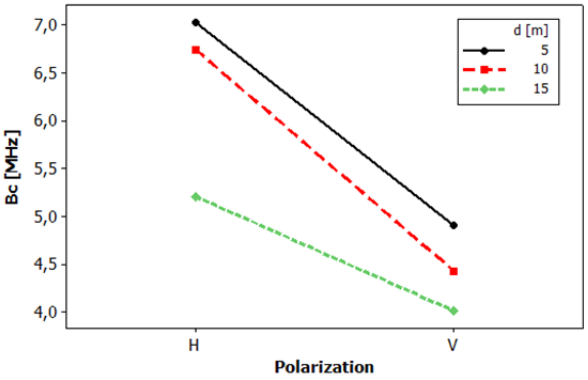

b) Interaction plot between polarization and distance for B_c

Figure 10. Main effects and interactions for B_c.

that while distance and polarization are indeed statistically significant as a cause for variations observed in experimental data ($p < 0.1\%$), interaction cannot be considered significant unless an error probability of at least 20% is accepted. However, the low value of the R^2_{adj} statistics (R^2_{adj} = 27%) tells that only about 27% of the variability in experimental data can be explained by the linear model including distance, polarization and their interaction. More factors should therefore be included in the model. This is not unexpected at all, since propagation in such a complex scenario as a train car is not only ruled by polarization and distance between transmitting and receiving systems.

Furthermore, it is necessary to verify that hypotheses for applicability of the ANOVA methodology are satisfied.

Table 2. Sample mean and sample variance for $\overline{\tau}$ and τ_{rms}.

Dist.	Pol.	$\overline{\tau}$		τ_{rms}	
		$\overline{x}$	s^2	$\overline{x}$	s^2
5	V	28.05	23.23	16.77	23.43
10		51.07	61.78	20.31	23.33
15		63.91	49.84	21.63	39.56
5	H	22.44	10.96	12.51	13.03
10		40.78	9.92	15.24	18.15
15		62.69	65.61	18.64	42.25

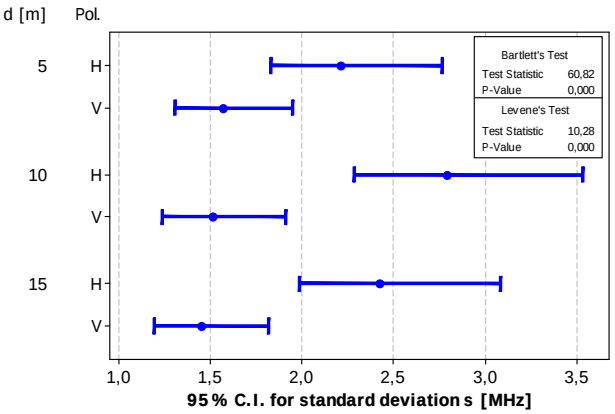

a) 95% confidence intervals for standard deviations

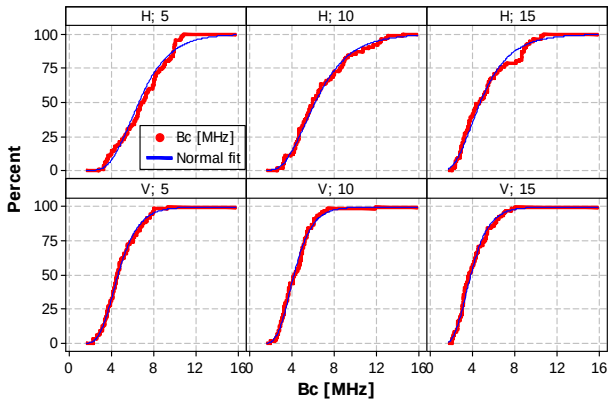

b) Experimental CDF's and log-normal fit

Figure 11. Validation of ANOVA hypothesis for B_c.

Figure 8 shows results of such validation. In Figure 8.a we see that although variances σ^2 can be assumed to be equal between horizontal and vertical polarization at a given distance, they cannot be considered to be equal in general assuming either normal (Bartlett's test) or continuous distributions (Levene's test). In Figure 8.b it is shown that the hypothesis of normal distribution of data for each combination of the input factors, unlike expected [24], is only verified for 10 m separation. Both conditions pose a limit to the validity of results of ANOVA although the very small p-values associated to the effect of distance and polarization may compensate for it.

To further test validity of results, the non-parametric Kruskal-Wallis test has been applied. It is equivalent to a one-way ANOVA, therefore interaction of factors cannot be determined. It does not require normality of data but does rely on equal variances assumption. By application of the test on τ_{rms} it turns out that both distance and polarization are significant at $p < 0.1\%$, confirming the aforementioned outcomes from ANOVA. It must be said however that variances as a function of distance cannot be considered equal ($p < 0.1\%$) while they can be considered equal as a function of polarization (Levene's test, p = 46.9%).

3.4. Coherence bandwidth B_c

Coherence bandwidth B_c is the frequency separation at which the frequency correlation function crosses a certain level c. Typical values of c are 0.9 and 0.5 [23].

Figure 9**Erro! A origem da referência não foi ncontrada.** shows a typical behavior of such functions for each polarization and distance. It must be noted that oscillations in the curves are caused by the multipath propagations and directly related to the amplitude of τ_{rms}. In Table 4 the sample mean and the sample variance of B_c for each configuration are reported.

Figure 10.a shows the main effects of distance and polarization on B_c, while Figure 10.b shows the interaction plot between the two quantities. Figure 10.a shows that on average, the two polarizations cause a significant change in the amplitude of B_c, namely the vertical polarization typically presents a lower value. Again, this may be due to the different boundary conditions encountered by vertically and horizontally polarized waves. The plot on the right of Figure 10.a shows that at greater distances the coherence bandwidth decreases, in accordance to the increase of the delay spread shown in Figure 7 and the behavior shown in Figure 9. The interaction plot in Figure 10.b shows that the reduction in B_c when the distance changes between 5 m and 15 m is slightly different for the two polarizations. The interaction plot therefore seems to indicate that there is small interaction between the two factors.

Again, for further analysis the analysis of variance (ANOVA) was run on experimental data. Results show that while distance and polarization are indeed statistically significant as a cause for variations observed in experimental data ($p < 0.1\%$), interaction can be considered significant at a level of 3.6%. Like for τ_{rms} the value of the R^2_{adj} statistics (R^2_{adj} = 23%) suggests that to explain

Table 3. Parameters of linear regression τ_{rms} vs $\bar{\tau}$.

Dist.	Pol.	α	β
5	V	1.63	0.54
10		-0.07	0.40
15		-16.36	0.59
5	H	-9.19	0.83
10		-29.16	1.09
15		-21.08	0.63

Table 4. Sample mean and sample variance for B_c.

Dist.	Pol.	$\bar{\tau}$	
		$\bar{x}$	s^2
5	V	4.92	2.47
10		4.44	2.28
15		4.02	2.10
5	H	7.03	2.21
10		6.75	4.88
15		5.21	5.90

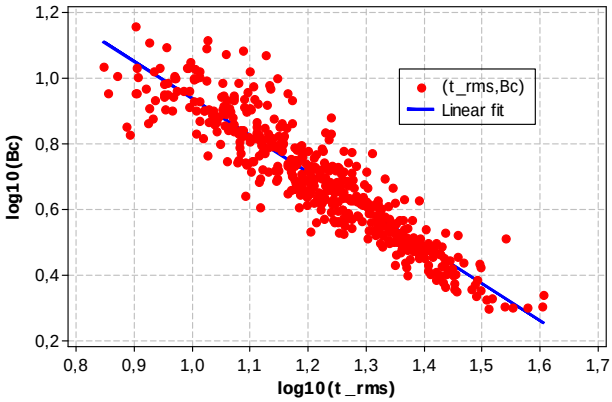

a) overall behavior of B_c vs. τ_{rms}

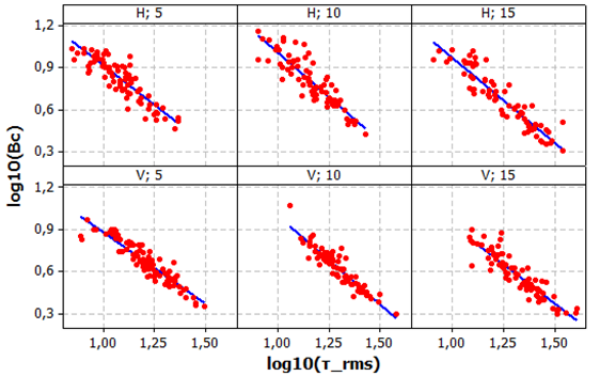

a) B_c vs. τ_{rms} for each combination of input factors

Figure 12. B_c vs. τ_{rms}.

variability in experimental data more factors should be included in the model. Again, this is expected just like for τ_{rms}, for the same reasons.

Validation of the hypotheses for applicability of the ANOVA methodology is shown in Figure 11. Figure 11.a shows that although variances σ^2 can be assumed to be equal at each polarization for the different distances, they cannot be considered to be equal in general assuming either normal (Bartlett's test) or continuous distributions (Levene's test). As for normality of B_c's data, it must be said that there is no evidence in scientific literature about a specific distribution. We found (see Figure 11.b) that the best fit is with a lognormal CDF in all cases except for the horizontal

Table 5. Values and 95% confidence intervals for *a* and *b*.

Dist.	Pol.	a		b	
		value	95 % C.I.	value	95 % C.I.
5	V	1,90	1,79; 2,01	1,02	0,93; 1,11
10		2,28	2,13; 2,43	1,28	1,16; 1,39
15		2,06	1,92; 2,21	1,13	1,02; 1,24
5	H	2,03	1,89; 2,18	1,12	0,99; 1,25
10		2,28	2,11; 2,45	1,27	1,13; 1,42
15		2,16	2,02; 2,30	1,20	1,08; 1,31
Overall		2,06	2,01; 2,12	1,13	1,08; 1,17

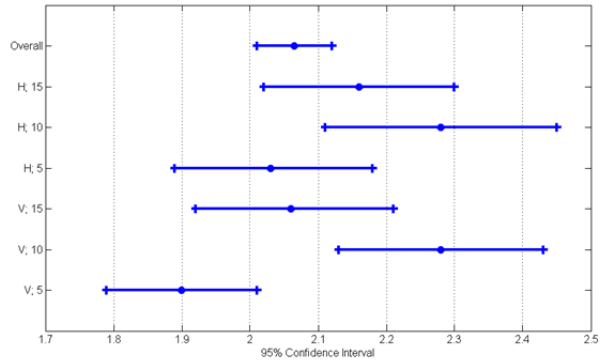

a) 95% confidence intervals for parameter *a*

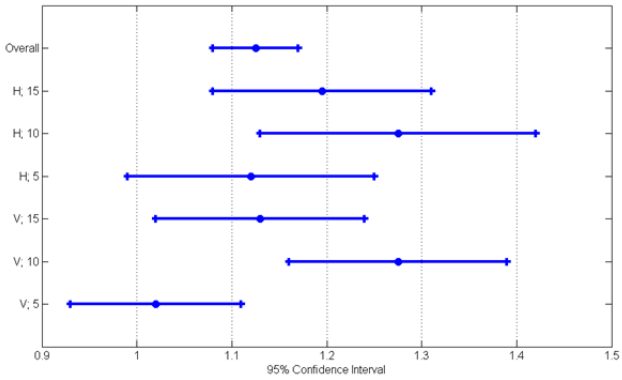

b) 95% confidence intervals for parameter *b*

Figure 13. 95% confidence interval for *a* and *b*.

polarization at 5 and 15 m. Like for delay spread, both conditions pose a limit to the validity of results of ANOVA, although the very small *p*-values associated to the effect of distance and polarization may compensate for it.

The non-parametric Kruskal-Wallis test has been applied also to B_c data. Again, results show that both distance and polarization are significant at $p < 0.1\%$. In this case, however, variances as a function of distance can be considered equal (Levene's test, $p = 29\%$) while they cannot be considered equal ($p < 0.1\%$) as a function of polarization.

3.5. Coherence bandwidth B_c vs. delay spread τ_{rms}

Often in literature the functional relation between B_c and τ_{rms} is identified by the following expression [23]:

$$B_c = \frac{1}{50\tau_{rms}} \tag{6}$$

by the more generic model [25]:

$$B_c = \frac{\alpha}{\tau_{rms}} \tag{7}$$

or by an even more generic one

Table 6. Values of ρ.

Overall	Hor. 5 m	Hor. 10 m	Hor. 15 m	Vert. 5 m	Vert. 10 m	Vert. 15 m
91.2%	88.0%	89.4%	92.6%	92.5%	93.0%	91.5%

$$B_c = \frac{\alpha}{\tau_{rms}^b} \quad (8)$$

in agreement with [26] and [27].

Values of the coherence bandwidth B_c versus the *rms* delay spread τ_{rms} are shown in Figure 12 together with the linear fit: the log-log representation changes eq. (4) to:

$$\log B_c = \log \frac{\alpha}{\tau_{rms}^b} = a - b \log \tau_{rms} \ . \quad (9)$$

In Figure 12.a regression has been applied to all available data, while in Figure 12.b each combination of polarization and distance has been considered separately. Values for *a* and *b*, and their 95% confidence intervals are shown in Table 5 and in Figure 13. Values are typically compatible, although the configuration at d = 5 m with vertical polarization does not overlap to the other intervals.

The large values of the correlation coefficient ρ reported in Table 6 for measurement data in both Figure 12.a and Figure 12.b show that τ_{rms} and B_c are strongly correlated and that their relationship is very close to a linear function.

4. CONCLUSION

The characterization of the propagation channel aboard train with a narrow-band methodology has been presented. Results show that the propagation law is very close to the free-space one, without significant differences between the propagation along the centerline and off-axis.

The delays spread and coherence bandwidth are strongly dependent on the polarization of the propagating signal and on the distance between transmitting and receiving antenna, horizontal polarization showing typically smaller spreads and thus larger coherence bandwidth. However, a detailed statistical analysis shows that variability in the data cannot be explained only by the contribution of polarization and distance, and therefore more factors should be included in the model. This is not unexpected given the very complex propagation environment. Finally, the parameters of the model describing B_c as a function of τ_{rms} typically do not depend on the propagation configuration.

REFERENCES

[1] D. Gallo, C. Landi, N. Pasquino, "An instrument for objective measurement of light flicker," Measurement, vol. 41, no. 3, pp. 334–340, April 2008.

[2] A. Mariscotti, A. Marrese, N. Pasquino, "Time and frequency characterization of radiated disturbances in telecommunication bands due to pantograph arcing", IEEE I2MTC - International Instrumentation and Measurement Technology Conference, Proceedings May 2012, pp. 2178-2182, doi: 10.1109/I2MTC.2012.6229310.

[3] A. Mariscotti, A. Marrese, N. Pasquino, "Experimental investigation on radiated emissions generated by pantograph arcing and their effects on telecommunication bands", 20th IMEKO World Congress 2012, Busan, Rep. of Korea, Sept. 2012, vol. 2, pp. 1175-1178.

[4] A. Mariscotti, A. Marrese, N. Pasquino, R. Schiano Lo Moriello, "Time and frequency characterization of radiated disturbance in telecommunication bands due to pantograph arcing," Measurement, Vol. 46, no. 10, pp. 4342-4352, Dec. 2013, doi: 10.1016/j./measurement.2013.04.054.

[5] V. Deniau, S. Dudoyer, M. Heddebaut, A. Mariscotti, A. Marrese, N. Pasquino, "Test bench for the evaluation of GSM-R operation in the presence of electric arc interference," Electrical Systems for Aircraft, Railway and Ship Propulsion (ESARS), Oct. 2012.

[6] S. Knorzer, M. Baldauf, T. Fugen, W. Wiesbeck, "Channel modelling for an ofdm train communications system including different antenna types," in Vehicular Technology Conference, 2006. VTC-2006 Fall. 2006 IEEE 64th, Sept. 2006, pp. 1–5.

[7] S. Knorzer, M. Baldauf, T. Fugen, W. Wiesbeck, "Channel analysis for an ofdm-miso train communications system using different antennas," in Vehicular Technology Conference, 2007. VTC-2007 Fall. 2007 IEEE 66th, 30 2007-oct. 3 2007, pp. 809 –813.

[8] J. Lu, G. Zhu, B. Ai, "Radio propagation measurements and modeling in railway viaduct area," in Wireless Communications Networking and Mobile Computing (WiCOM), 2010 6th International Conference on, Sept. 2010, pp. 1–5.

[9] R. He, Z. Zhong, B. Ai, J. Ding, "An empirical path loss model and fading analysis for high-speed railway viaduct scenarios," Antennas and Wireless Propagation Letters, IEEE, vol. 10, pp. 808–812, 2011.

[10] J. Lu, G. Zhu, C. Briso-Rodriguez, "Fading characteristics in the railway terrain cuttings," in Vehicular Technology Conference (VTC Spring), 2011 IEEE 73rd, may 2011, pp. 1–5.

[11] R. He, Z. Zhong, B. Ai, J. Ding, "Propagation measurements and analysis for high-speed railway cutting scenario," Electronics Letters, vol. 47, no. 21, pp. 1167–1168, 13 2011.

[12] N. Kita, T. Ito, S. Yokoyama, M.-C. Tseng, Y. Sagawa, M. Ogasawara, M. Nakatsugawa, "Experimental study of propagation characteristics for wireless communications in high-speed train cars," in Antennas and Propagation, 2009. EuCAP 2009. 3rd European Conference on, march 2009, pp. 897 –901.

[13] T. Ito, N. Kita, W. Yamada, M.-C. Tseng, Y. Sagawa, M. Ogasawara, M. Nakatsugawa, T. Sugiyama, "Study of propagation model and fading characteristics for wireless relay system between long-haul train cars," in Antennas and Propagation (EUCAP), Proceedings of the 5th European Conference on, April 2011, pp. 2047–2051.

[14] W. Dong, G. Liu, L. Yu, H. Ding, J. Zhang, "Channel properties of indoor part for high-speed train based on wideband channel measurement," in Communications and Networking in China (CHINACOM), 2010 5th International ICST Conference on, aug. 2010, pp. 1–4.

[15] E. Balboni, J. Ford, R. Tingley, K. Toomey, J. Vytal, "An empirical study of radio propagation aboard naval vessels," in Antennas and Propagation for Wireless Communications, 2000 IEEE-APS Conference on, 2000, pp. 157–160.

[16] E. L. Mokole, M. Parent, T. T. Street, E. Tomas, "RF propagation on ex-uss Shadwell," IEEE Conf.Anten.Propag.Wireless Commun., pp. 153–156, 2000.

[17] D. R. J. Estes, T. B. Welch, A. A. Sarkady, H. Whitesel, "Shipboard radio frequency propagation measurements for wireless networks," in Proceedings - IEEE Military Communications Conference MILCOM, vol. 1, 2001, pp. 247–251.

[18] P. Nobles, R. Scott, "Wideband propagation measurements onboard HMS Bristol," in Proceedings - IEEE Military

Communications Confer-ence MILCOM, vol. 2, 2003, pp. 1412–1415.

[19] P. Bifulco, A. Liccardo, A. Mariscotti, A. Marrese, N. Pasquino, R. Schiano Lo Moriello, "Wide-band and Narrow-band Characterization of the Propagation Channel in Trains," International Review of Electrical Engineering (IREE), Vol. 8, Is. 5, Oct. 2013, pp. 1467-1472.

[20] A. Mariscotti, A. Marrese, N. Pasquino, R. Schiano Lo Moriello, "Characterization of the propagation channel aboard trains," in 19th IMEKO TC-4 Symposium, Proceedings of, Barcelona, Spain, July 2013, pp. 339-344.

[21] L. Angrisani, M. D'Apuzzo, D. Grillo, N. Pasquino, R. Schiano Lo Moriello, "A new time-domain method for frequency measurement of sinusoidal signals in critical noise conditions," Measurement, Vol. 49, Is. 1, March 2014, pp. 368-381, doi: 10.1016/j.measurement.2013.11.034.

[22] J. Turkka, M. Renfors, "Path loss measurements for a non-line-of-sight mobile-to-mobile environment," in ITS Telecommunications, 2008. ITST 2008. 8th International Conference on, Oct., pp. 274–278.

[23] T. Rappaport, Wireless Communications: Principles and Practice. Prentice Hall PTR, 1996.

[24] H. Hashemi, D. Tholl, "Analysis of the RMS delay spread of indoor radio propagation channels," Communications, 1992. ICC '92, Conference record, SUPERCOMM/ICC '92, Discovering a New World of Communications., IEEE International Conference on, vol.2, pp.875-881, 14-18 Jun 1992.

[25] G. Morrison, M. Fattouche, H. Zaghloul, "Statistical analysis and autoregressive modeling of the indoor radio propagation channel," in Universal Personal Communications, 1992. ICUPC '92 Proceedings., 1st International Conference on, 1992, pp. 04.03/1–04.03/5.

[26] M.S. Varela, M.G. Sanchez, "RMS delay and coherence bandwidth measurements in indoor radio channels in the UHF band," Vehicular Technology, IEEE Transactions on, vol. 50, no. 2, pp.515,525, Mar 2001.

[27] S. Howard, K. Pahlavan, "Measurement and analysis of the indoor radio channel in the frequency domain," Instrumentation and Measure-ment, IEEE Transactions on, vol. 39, no. 5, pp. 751–755, 1990.